The dissociation of vibrationally excited CH_3OSO radicals and their photolytic precursor, methoxysulfinyl chloride

Bridget W. Alligood,[1] Caroline C. Womack,[1] Daniel B. Straus,[1] Frances R. Blase,[2] and Laurie J. Butler[1,a)]

[1]*The James Franck Institute and Department of Chemistry, University of Chicago, Chicago, Illinois 60637, USA*

[2]*Department of Chemistry, Haverford College, Haverford, Pennsylvania 19041, USA*

(Received 17 February 2011; accepted 19 April 2011; published online 18 May 2011)

The dissociation dynamics of methoxysulfinyl radicals generated from the photodissociation of $CH_3OS(O)Cl$ at 248 nm is investigated using both a crossed laser – molecular beam scattering apparatus and a velocity map imaging apparatus. There is evidence of only a single photodissociation channel of the precursor: S-Cl fission to produce Cl atoms and CH_3OSO radicals. Some of the vibrationally excited CH_3OSO radicals undergo subsequent dissociation to $CH_3 + SO_2$. The velocities of the detected CH_3 and SO_2 products show that the dissociation occurs via a transition state having a substantial barrier beyond the endoergicity; appropriately, the distribution of velocities imparted to these momentum-matched products is fit by a broad recoil kinetic energy distribution extending out to 24 kcal/mol in translational energy. Using 200 eV electron bombardment detection, we also detect the CH_3OSO radicals that have too little internal energy to dissociate. These radicals are observed both at the parent CH_3OSO^+ ion as well as at the CH_3^+ and SO_2^+ daughter ions; they are distinguished by virtue of the velocity imparted in the original photolytic step. The detected velocities of the stable radicals are roughly consistent with the calculated barriers (both at the CCSD(T) and G3B3 levels of theory) for the dissociation of CH_3OSO to $CH_3 + SO_2$ when we account for the partitioning of internal energy between rotation and vibration as the CH_3OSOCl precursor dissociates.
 [doi:10.1063/1.3589273]

I. INTRODUCTION

The oxidation of dimethyl sulfide (DMS) has been shown to be a major source of sulfur dioxide (SO_2) in the troposphere.[1] Understanding the competition between both the rates of formation and dissociation of various adducts, along with the reactions of these adducts with other atmospheric species in the overall oxidation mechanism, is key to interpreting the observed temperature-dependent branching of DMS to stable end products.[2,3] There are two isomers of the adduct of methyl radicals and SO_2, methylsulfonyl (CH_3SO_2) and methoxysulfinyl (CH_3OSO).[3] An investigation of the methylsulfonyl radical and its subsequent unimolecular dissociation to $CH_3 + SO_2$ was previously reported by our group.[4,5] In that study, we compare our results to other published reports, both experimental and theoretical.[6–9]

Previous theoretical work has also been done on the CH_3OSO radical. Frank and Turecek, in 1999, predicted that this radical dissociates to $CH_3 + SO_2$ solely through isomerization to CH_3SO_2.[10] These results were obtained using Rice-Ramsperger-Kassel-Marcus theory, based upon a calculated isomerization barrier of 23.4 kcal/mol – approximately 10 kcal/mol lower than the barrier to direct dissociation of CH_3OSO to CH_3 and SO_2. In contrast, Zhu and Bozzelli's calculated barrier at the G3(MP2) level of theory suggested that CH_3OSO can dissociate directly without isomerization, having a barrier to direct dissociation ~20 kcal/mol lower than the isomerization barrier.[11] Our previous work[5] revealed that the isomerization barrier reported by Frank and Turecek was based on a spurious transition state; in that paper, we recalculated the transition state energetics with the G2(MP2) level of theory – the level of theory used in the Frank and Turecek work – and found that the actual energetic barrier to isomerization to CH_3SO_2 was indeed much higher (~21 kcal/mol) than the barrier out to $CH_3 + SO_2$. Thus, while the discrepancy between these two papers can easily be explained, their disagreement still highlights a fundamental need to have accurate and reliable electronic structure methods available.

This work investigates the photodissociation of methoxysulfinyl chloride, $CH_3OS(O)Cl$, at 248 nm, as well as the subsequent dissociation of the vibrationally excited CH_3OSO radicals that are formed. Unlike CH_3SO_2, which undergoes dissociation to $CH_3 + SO_2$ via a "loose" transition state having a negligible barrier beyond the 14 kcal/mol endoergicity, theoretical calculations reveal that the CH_3OSO radicals do so with a substantial barrier (30.7 kcal/mol for the *syn*-isomer and 28.7 for the *anti*-isomer, based on Lau's coupled-cluster single double triple [CCSD(T)] results[4]). We would expect this to result in CH_3 and SO_2 dissociation products with more substantial recoil velocities imparted as a result of the repulsive forces in the exit channel. The data presented herein resolve the unimolecular dissociation of the nascent radicals to $CH_3 + SO_2$ and show that some of the CH_3OSO radicals remain undissociated due to their low internal energy.

a)Author to whom correspondence should be addressed. Electronic mail: L-Butler@uchicago.edu.

The work presented herein offers key data for validating emerging electronic structure calculations of these important radical intermediates. This is particularly useful given the challenge that sulfur-containing radicals present to current electronic structure methods. Our previous work highlighted some of the conflicting published data; Zhu and Bozzeli concluded their work with the assertion that, while G3 methods gave good energetics, the CCSD(T) method was unreliable.[11] Ratliff *et al.* presented a basis set convergence analysis[4] showing that good energetics for the dissociation barrier to $CH_3 + SO_2$ are obtained with the CCSD(T) method if one includes not only inner polarization functions (tight-*d* functions) in the basis functions for the sulfur atom, as suggested in seminal work by Martin,[12] but also core-valence and relativistic corrections.

II. METHODS

A. Preparation of methoxysulfinyl chloride ($CH_3OS(O)Cl$)

Methoxysulfinyl chloride ($CH_3OS(O)Cl$) was synthesized according to a modified procedure from a previously published report.[13] All glassware was flame-dried and cooled under vacuum prior to use. Thionyl chloride ($SOCl_2$, 99.5%) was purchased from Sigma Aldrich and used without further purification. Anhydrous methanol was prepared by distillation over Na metal under an inert atmosphere of Ar gas.

Thionyl chloride (26 g, 200 mmol) was added to a 100 ml round bottom flask equipped with a stir bar and pressure-equalizing addition funnel with a Teflon stopcock. The solution was stirred at room temperature under an inert atmosphere of Ar, and anhydrous methanol (6.4 g, 200 mmol) was slowly added, drop-wise, via the addition funnel. After the addition was complete, the resulting pale yellow solution was stirred at room temperature for 48 h, during which time it became dark yellow in color. The flask was then equipped for vacuum distillation under reduced pressure (100 mmHg). The product was isolated as a colorless liquid and stored in a sealed round bottom flask at 10 °C under an Ar atmosphere. ^{1}H NMR was used to verify that the desired product was formed; in $CDCl_3$, the $CH_3OS(O)Cl$ isomer has a chemical shift at 4.0 ppm. A representative spectrum is given in the supplemental material.[14] Confirmed impurities in the synthesized product include the following: the unreacted $SOCl_2$ reagent and dimethyl sulfite ($CH_3OS(O)OCH_3$), the product resulting from the addition of 2 methanol molecules to a single molecule of thionyl chloride; the latter has a peak in the ^{1}H NMR spectrum at 3.6 ppm.[15]

B. Experimental method – Scattering apparatus

Upon photodissociation at 248 nm, methoxysulfinyl chloride ($CH_3OS(O)Cl$) yields the CH_3OSO radical. We use a crossed laser-molecular beam apparatus to measure the distribution of velocities imparted to the Cl atoms upon photodissociation. The momentum-matched CH_3OSO radicals are formed under collision-free conditions to facilitate the characterization of their internal energy distribution and subsequent dynamics. We can detect both the nascent radicals formed with a low enough internal energy to be stable to dissociation as well as the dissociation products of the higher internal energy radicals.

For these experiments, we expand the continuous (not pulsed) molecular beam through an orifice of diameter 0.15 mm; we heat the nozzle to 80 °C. We note that the $CH_3OS(O)Cl$ synthesized product was extremely reactive with metals, corroding nickel, copper, and even stainless steel. Thus, where feasible, we replaced metal parts with Teflon ones; this included transfer lines, joints, and valve bodies. Because we were unable to replace our stainless steel nozzle with a Teflon (or glass) one, we used a polymer coating (Cytonix FluoroPel™ 502A-FS) to deter corrosion of the nozzle body. The Fluoropel™ polymer was applied by dipping the nozzle into the solution and heating to about 90 °C for 10 min.

We created the molecular beam by seeding the equilibrium vapor pressure of $CH_3OS(O)Cl$ at −5 °C in He to a total pressure of 400 Torr. The molecular beam passes through two skimmers before entering the main chamber. There, it intersects the output of a pulsed 248 nm laser (using the KrF transition of an unpolarized Lumonics PM-848 excimer laser). We focus the laser pulses down to a beam spot with a ~6 mm^2 cross-sectional area in the interaction region. Over the course of the experiment, we maintained a laser power of roughly 57 mJ/pulse.

The laser light propagates along an axis that is perpendicular to the plane defined by the molecular beam and the detector axis, resulting in light that is unpolarized in the scattering plane. The neutral photodissociation products scatter from the interaction region with velocities determined by the vector sum of the molecular beam velocity and the recoil velocity imparted during the photodissociation. Those scattering into the 1.5° acceptance angle of the differentially pumped detector travel 45.0 cm to an electron bombardment ionizer, where they are ionized by 200 eV electrons.[16] High voltage lenses accelerate and focus these ions toward the entrance of a quadrupole mass spectrometer, where they are mass-selected and detected using a Daly detector.[17] The resultant voltage pulses are counted by a multi-channel scaler; the signal is proportional to the number of ions at each mass to charge ratio, detected as a function of time after the dissociating light pulse. We accumulate the signal in 2 μs channels, and we plot all data and fit points at the end of each time window. Upon subtraction of the calibrated ion flight time, calculated using the apparatus' measured ion flight constant of 4.5 μs amu$^{-1/2}$, forward convolution fitting of the time-of-flight (TOF) spectrum determines the distribution of energies imparted to relative product translation during the dissociation, E_T.

To characterize the molecular beam, we align the source along the detector axis and raise a 300 Hz chopper wheel into the beam. To calibrate the neutral flight path, we use a He beam and an unheated nozzle. The number density distribution of velocities in the molecular beam typically peaks at 1400 m/s, with a FWHM of 10%. To measure the velocities of the neutral photofragments reported in this paper, the molecular beam source is rotated to different angles in the plane containing the beam and detector axis, which is

perpendicular to the laser beam propagation direction. The angle at which data are acquired is indicated in the upper right corner of all presented spectra.

Beyond the data presented herein, we also looked for signal at m/e = 32 (S^+, O_2^+) m/e = 48 (SO^+), m/e = 83 ($SOCl^+$), m/e = 95 ($CH_3OS(O)O^+$), m/e = 99 ($OSOCl^+$), m/e = 110 ($CH_3OS(O)OCH_3^+$), and m/e = 114 ($CH_3OS(O)Cl^+$); all spectra are given in the supplemental material.[14] The data taken at m/e = 114 had no signal above the noise after 1×10^6 laser shots. The data at m/e = 83, 95, 99, and 110 were taken in attempts to verify the presence of impurities in the sample. For m/e = 95, 99, and 110, little or no signal appeared above the noise after 1×10^6 laser shots. The signal observed at m/e = 83, however, did confirm the presence of $SOCl_2$. The absorption cross section for thionyl chloride is on the order of 10^{-18} cm^2/molecule,[18] so the presence of this impurity made a substantial contribution to the signal at mass-to-charge ratios common to both the $SOCl_2$ and the $CH_3OS(O)Cl$ photodissociation products. To resolve this, we also took data with a pure $SOCl_2$ beam (seeded in He); doing so allowed us to precisely subtract the contribution from $SOCl_2$ dissociation products and reveal the signal resulting solely from $CH_3OS(O)Cl$ photodissociation. For those experiments using the pure $SOCl_2$ beam, the number density distribution of velocities in the molecular beam typically peaks at 1100 m/s, with a FWHM of 9%. For these experiments involving pure $SOCl_2$, we present the time-of-flight spectrum obtained for m/e = 35 (Cl^+), but not for other masses at which signal was obtained: m/e = 32 (S^+), m/e = 48 (SO^+), m/e = 69 ($S^{37}Cl^+$), and m/e = 83 ($SOCl^+$). Unlike the m/e = 35 spectrum, which contained a substantial amount of signal resulting from the photodissocation of $CH_3OS(O)Cl$, all of the other spectra were overwhelmingly composed of signal from the photodissociation of $SOCl_2$. The photodissociation of $SOCl_2$ has been well characterized in previous experiments,[18–22] so we do not show these spectra in this paper; we refer the interested reader to the supplemental material.[14]

C. Experimental method – Imaging apparatus

The velocity map imaging apparatus used in this work has been described previously,[23–26] so only a brief description and modifications are provided here. We maintain a similar molecular beam seed ratio to the experiments taken in the scattering apparatus, using the equilibrium vapor pressure of $CH_3OS(O)Cl$ at 0 °C seeded in He to a total stagnation pressure of 500 Torr. We expand the beam through a General Valve Iota One pulsed valve, with an orifice diameter of 0.8 mm, and we heat the nozzle to 80 °C. After passing through a skimmer, the molecules are photodissociated with a vertically – polarized 248 nm beam generated by a GAM (EX10F/300) KrF laser. We focus the beam such that the focal point lies roughly 1 cm beyond the intersection of the laser with the molecular beam. We maintain pulse energies that are typically less than 1 mJ/pulse.

The photofragments are ionized by 118 nm (10.5 eV) light, fired ~40 ns after the photodissociation laser, which we generate[4] by tripling the 355 nm output beam from a pulsed Nd:YAG laser (Continuum Surelite I-20). Repeller and extractor plates, with a voltage ratio of 1.4:1, serve to accelerate the spherically expanding cloud of ions down an ~577 mm grounded time-of-flight tube towards the detector (Burle 3040FM). The detector consists of a position-sensitive Chevron microchannel plate assembly (MCP) coupled to a P20 phosphor screen. We pulse the voltage on the front plate of the MCP to −750 V in order to coincide with the arrival time of ions having the desired mass-to-charge ratio. The phosphor screen is maintained at 3.3 kV above the potential of the rear MCP plate. A cooled charge-coupled device (CCD) camera (La Vision Imager 3), with a standard 35 mm lens, records images of the ions. We process the obtained images using the ion-counting method, and the raw images are symmetrized about the vertical and horizontal axes in the data analysis.

We present data obtained from images taken at m/e = 15 (CH_3^+) and m/e = 79 (CH_3OSO^+), and include in the supplemental material[14] images taken at m/e = 32 (S^+), m/e = 34 ($^{34}S^+$), m/e = 48 (SO^+), m/e = 64 (SO_2^+), m/e = 83 ($SOCl^+$), and m/e = 110 ($CH_3OS(O)CH_3^+$). The m/e = 34 signal resulted in an identical speed distribution to the m/e = 32 (S^+) signal, so we attribute it to the sulfur isotope, ^{34}S. The m/e = 110 was only qualitatively used to confirm the presence of the $CH_3OS(O)OCH_3$ impurity, and m/e = 83 was used to verify the presence of $SOCl_2$ (which dissociates to SOCl and Cl at 248 nm). The very weak signal at m/e = 64 in the imaging lab must be from multiphoton ionization; the ionization energy of neutral SO_2 is above 10.5 eV (12.3 eV by photoelectron spectroscopy[27]).

In addition to these spectra taken with 10.5 eV photoionization, we also use 2+1 resonance-enhanced multiphoton ionization to detect the Cl photofragments that result from S-Cl bond fission. We use 235.33 nm ($4p^2D_{3/2} \leftarrow 3p^2P_{3/2}$) and 235.20 nm ($4p^2P_{1/2} \leftarrow 3p^2P_{1/2}$) photons to state-selectively ionize $Cl(^2P_{3/2})$ and $Cl(^2P_{1/2})$, respectively, as detailed in Ref. 4. These images and associated spectra are given in the supplementary material.[14]

III. RESULTS AND ANALYSIS

A. Thionyl chloride ($SOCl_2$)

As mentioned in the Methods section, there are a few impurities present in the synthesized product; the most notable of these are the unreacted thionyl chloride ($SOCl_2$) reagent and dimethyl sulfite ($CH_3OS(O)OCH_3$), the product resulting from the addition of two methanol molecules to a single molecule of thionyl chloride. The former will be discussed in this section, and we will return to a brief discussion on the latter in Sec. III E.

The unreacted reagent provided the most concerning source of contamination, as the absorption cross section of $SOCl_2$ is on the order of 10^{-18} cm^2/molecule at 248 nm.[18] The reaction product was distilled under vacuum, and the liquid, maintained at −5 °C, was degassed prior to introduction into the reaction chamber. Both measures were taken in attempts to separate the $CH_3OS(O)Cl$ products from the $SOCl_2$ products. Nevertheless, substantial signal from the photodis-

sociation of $SOCl_2$ was apparent in the data. To resolve this problem, we took scattering data on $SOCl_2$ (pure, seeded in He) and subtract the associated signal from the data taken on the synthesized product. Previous papers[18–22] on the photodissociation of $SOCl_2$ at 248 nm were helpful in fitting our observed signal; we only needed to rescale the contribution from multiphoton dissociation and fit the signal attributed to the dissociation of molecular clusters. The top frame of Fig. 1 shows the observed m/e = 35 (Cl^+) signal resulting from the photodissociation of $SOCl_2$ at 248 nm. Using the $P(E_T)$'s reported in Baum *et al.*,[19] we get the overall fit shown in solid black line in that frame. The contributions to this fit include signal resulting from the following three processes:

$$SOCl_2 + h\nu \rightarrow Cl + SOCl, \quad (1)$$

where both the signal resulting from the Cl product directly (peaking around 150 μs) and that resulting from dissociative ionization of the momentum-matched SOCl partner (peaking around 230 μs) are shown in dotted black line,

$$SOCl + h\nu \rightarrow Cl + SO, \quad (2)$$

whereby the SOCl product formed in process (1) absorbs another 248 nm photon and further dissociates to Cl + SO (shown in dashed gray line), and

$$SOCl_2 + h\nu \rightarrow Cl_2 + SO, \quad (3)$$

with signal resulting from dissociative ionization of the Cl_2 photoproduct given in solid gray line.

The slower signal, arriving after 200 μs, is unfit by the above three processes. The Baum *et al.* paper generally attributed this signal, in its entirety, to the dissociative ionization of molecular clusters ($(SOCl_2)_n$) in the beam. We also note that this is likely; after accounting for the flight time through the ionizer at the different mass-to-charge ratios, this signal also appears at both m/e = 32 (S^+) and m/e = 48 (SO^+). We do note, however, that the relative ratios (faster portion:slower portion) of these contributors were different in the three spectra (6.2 for the m/e = 32 spectra, 4.3 for the m/e = 48 spectra, and 3.55 for the m/e = 35 spectra, all given in the supplemental material[14]). For our experiments, we fit this slowest signal using two different recoil translational energy distributions; the predictions based on these distributions are both shown in dashed black line, one peaking around 300 μs with the other around 350 μs. We chose these two $P(E_T)$'s via an iterative process that resulted in the ability to predict the signal in all three spectra by altering only the relative amounts of the two $P(E_T)$'s. The predicted signal based on these two $P(E_T)$'s are given in the upper and middle frame of Fig. 1. The m/e = 32 and m/e = 48 spectra, with their corresponding fits, are given in the supplemental material for comparison.

B. S-Cl bond fission in the $CH_3OS(O)Cl$ precursor, yielding CH_3OSO radicals and Cl

The bottom frame of Fig. 1 shows the portion of the time-of-flight spectrum taken at m/e = 35 (Cl^+) resulting from the photodissociation of $CH_3OS(O)Cl$. This spectrum is obtained by subtracting the Cl^+ signal obtained in the photodissociation of pure $SOCl_2$, described in the preceding

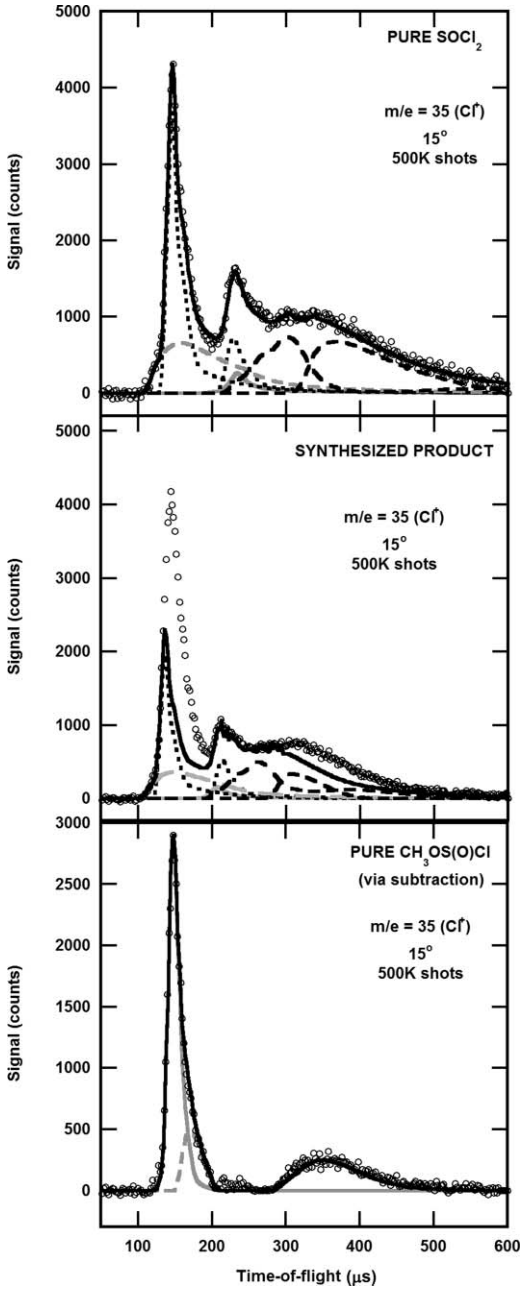

FIG. 1. Time-of-flight spectra at m/e = 35 (Cl^+) from the photodissociation of methoxysulfinyl chloride, $CH_3OS(O)Cl$, and thionyl chloride, $SOCl_2$. The three frames show explicitly how the Cl^+ signal resulting from the photodissociation of pure thionyl chloride was subtracted from our data to derive, in the lower frame, the net Cl^+ signal resulting solely from $CH_3OS(O)Cl$ photodissociation. The data are shown in open circles, and the total forward convolution fits to the data are shown in solid black line. The upper frame shows the fit to the Cl^+ signal resulting from the photodissociation of a pure thionyl chloride beam at 248 nm. The contributions to that fit are described in the text. The fit obtained was then scaled in the middle frame to the Cl^+ signal resulting from the synthesized $CH_3OS(O)Cl$ product (which contained unreacted $SOCl_2$ as a contaminant). The remaining signal, that unfit by the scaled $SOCl_2$ fit, is shown in the lower frame; it is the Cl^+ signal resulting from the photodissociation of $CH_3OS(O)Cl$. In that frame, the signal from Cl atoms produced in the S-Cl bond fission of methoxysulfinyl chloride at 248 nm is shown in solid and dashed gray lines (differentiating whether the Cl atom's CH_3OSO momentum matched product is stable or unstable, respectively). This fit is used to derive the total recoil kinetic energy distribution shown in Fig. 2. The bottom frame clearly reveals a contribution, peaking near 350 μs, from the photodissociation of molecular clusters in the beam; this distribution, shown in dashed black line, was used to identify all cluster contributions at other mass-to-charge ratios.

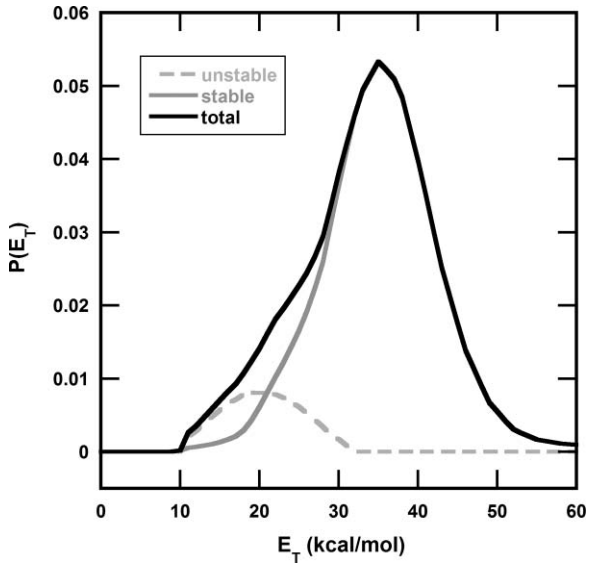

FIG. 2. The total recoil kinetic energy distribution, $P(E_T)$, derived from forward convolution fitting of the data taken at m/e = 35 (Cl^+), as shown in the lower frame of Fig. 1. We identified the portion of the $P(E_T)$ (shown in solid gray line) that results in radicals stable to subsequent dissociation to $CH_3 + SO_2$ from the image shown in Fig. 4, which gives the speed distribution of the stable CH_3OSO radicals. The remaining portion of the $P(E_T)$, shown in dashed gray line, gives radicals with enough vibrational energy to dissociate. The $P(E_T)$ is uncorrected for the speed dependence of the anisotropy.

subsection, from the total signal at Cl^+ shown in the middle frame. In the middle frame of Fig. 1, the scaled $SOCl_2$ fit is shown superimposed on the total Cl^+ data taken with the synthesized product; this signal again contains both the photodissociation products from the desired $CH_3OS(O)Cl$ precursor as well as from the $SOCl_2$ contaminant. The fit was subtracted from the overall signal to yield the m/e = 35 (Cl^+) signal from just $CH_3OS(O)Cl$ photodissociation (lower frame of Fig. 1),

$$CH_3OS(O)Cl + h\nu \rightarrow Cl + CH_3OSO. \quad (4)$$

We used forward convolution fitting of the signal between 100 and 200 μs to derive the total S-Cl bond fission recoil kinetic energy distribution, $P(E_T)$, shown in the dashed black line in Fig. 2. This fit is made of two parts: Cl atoms produced in conjunction with stable CH_3OSO radicals and Cl atoms produced in conjunction with CH_3OSO radicals formed with higher internal energy (and thus with enough energy to dissociate to $CH_3 + SO_2$); these contributions are shown in solid gray and dashed gray line, respectively. The solid gray line was obtained by considering the total recoil kinetic energy distribution of the momentum-matched stable m/e = 79 products observed in the imaging experiments; this will be discussed in detail in Sec. III D. Imaging experiments were also performed at m/e = 35; the overwhelming presence of the $SOCl_2$ contaminant, however, did not allow for conclusive arguments based on them. These images and spectra are given in the supplementary material.[14]

The slower signal peaking around 350 μs is attributed to the dissociation of molecular clusters ($(CH_3OS(O)Cl)_n$) in the beam. We use forward convolution fitting of this signal, where it is easy to distinguish and separate from other contributing signal sources, to derive a speed distribution associated with this cluster photodissociation. By correcting for the flight time through the ionizer, we are then able to predict the arrival time at all daughter ions. Because all spectra were taken under similar beam conditions, we use this speed distribution to fit the cluster contribution in all spectra in this paper. It is shown in dashed black line in all relevant figures (Figs. 6, 11, and 12, and the bottom frame of Fig. 1).

C. Predicted internal energy distribution of the CH_3OSO radicals

The internal energy distribution of all nascent radicals, both stable and unstable, can be predicted from energy conservation, using the total recoil kinetic energy distribution shown in Fig. 2; this distribution is derived from the measured Cl atom velocities and momentum conservation. For each measured recoil kinetic energy, E_T, we calculate the internal energy in the nascent CH_3OSO radicals from,

$$E_{int}(CH_3OSO) = h\nu + E_{precursor} - D_0(S-Cl) - E_{Cl} - E_T. \quad (5)$$

Here, the G3//B3LYP/6-311++g(3df,2p) value of 57.1 kcal/mol and 59.2 kcal/mol are the dissociation energies of the S-Cl bond, D_0, for the two different isomers – *syn* and *anti*, respectively; the same geometry is assumed for both the chlorinated precursor and the radical species. The photon energy, $h\nu$, is 114.9 kcal/mol, and the energy in spin-orbit excitation of the Cl atom product is denoted E_{Cl}. $E_{precursor}$ is the internal energy of the $CH_3OS(O)Cl$ precursor. It can be estimated by assuming that the rotational energy of the $CH_3OS(O)Cl$ molecules is effectively cooled in the supersonic expansion, but that the vibrational energy is characterized by a thermal distribution at the nozzle temperature. We thus estimate that both isomers have an average of 3.49 kcal/mol of internal vibrational energy. E_{Cl} is 0 kcal/mol for CH_3OSO radicals produced in conjunction with ground state $Cl(^2P_{3/2})$ atoms and 2.5 kcal/mol for radicals produced in conjunction with spin-orbit excited state $Cl(^2P_{1/2})$ atoms. As this small additional internal energy is within the resolution of our experiments and cannot be separately resolved, it will be included with that of the radicals for plots in this paper.

The E_{int} term in the equation above is comprised of rotational, vibrational, and electronic energy of the nascent CH_3OSO radical formed in the dissociation. The high recoil kinetic energy products resulting from this S-Cl bond fission process partition some amount of rotational energy to the departing CH_3OSO radical. Using the impulsive model described in Ratliff *et al.*,[28] and assuming excited state impulsive forces at the ground state equilibrium geometry, we calculate for the *syn* conformer an impact parameter, *b*, of 1.37 Å and a moment of inertia for the nascent rotating radical, *I*, of 75.3 amu Å^2. The rotational energy in the nascent radical, for each of the recoil kinetic energies E_T, for S-Cl bond fission measured in the experiment, is given by $E_{rot} = (\mu b^2/I)E_T = 0.61\ E_T$, where μ is the reduced mass of the dissociating

fragments. For the *anti* conformer, these values are $b = 1.59$ Å and $I = 119.1$ amu Å^2, yielding $(\mu b^2/I)E_T = 0.515\ E_T$.

Substituting $E_{vib} + E_{rot}$ for the E_{int} term in Eq. (5) and solving for E_{vib} gives

$$E_{vib}(CH_3OSO) = h\nu + E_{precursor} - D_0(S-Cl) - E_{Cl} - \left(1 + \frac{\mu b^2}{I}\right)E_T. \quad (6)$$

Using the predicted dissociation barrier of the *syn*-isomer (28.76 kcal/mol with G3B3[5] and 30.7 kcal/mol with CCSD(T)[4]) and *anti*-isomer (26.64[5] and 28.7 kcal/mol[4], respectively), along with the impulsive model predicting the amount of internal energy partitioned to rotation, we can use the fastest Cl atom velocities to predict the velocity spectrum and TOF spectrum of the stable CH_3OSO radicals. The results of this model are shown in the upper frame of Fig. 3. Accounting for the statistical thermal population of the two isomers (51:49 *syn*:*anti*), we get reasonably good agreement with the experimentally observed stable radical spectrum; this comparison is shown explicitly in the upper frame of Fig. 3.

D. Detecting the stable CH_3OSO radicals

For those S-Cl bond fission events partitioning the highest relative kinetic energy to the recoiling Cl atoms, the momentum-matched CH_3OSO radicals are formed with low internal energies, some below the predicted dissociation barrier to $CH_3 + SO_2$. In the experiments using the scattering apparatus, we saw good signal at m/e = 79 (CH_3OSO^+). Accounting for flight time through the ionizer, however, we also saw dissociative ionization of these radicals to m/e = 15 (CH_3^+) and m/e = 64 (SO_2^+); these contributions will be detailed in Sec. III F. The m/e = 79 time-of-flight spectrum obtained in the scattering experiments was itself further complicated by other contributing signal sources. These sources include the dissociative ionization of the $CH_3OS(O)O$ (mass 95) photofragment discussed later in Sec. III E as well as products resulting from the photodissociation of molecular clusters in the beam as discussed in Sec. III B. The data taken in the imaging lab, using 10.5 eV photoionization, is free from these other contributing signal sources. Thus, we can use the image obtained at m/e = 79 (see Fig. 4) to derive the speed distribution, P(v), of those CH_3OSO radicals with low enough vibrational energy to be stable to subsequent dissociation to $CH_3 + SO_2$. Only the CH_3OSO radicals that are momentum matched to the highest velocity Cl atoms are formed with low enough vibrational energies to lie below the dissociation barrier out to $CH_3 + SO_2$. The P(v) obtained is shown in the upper frame of Fig. 5. The m/e = 79 data, taken with a vertically polarized 248 nm laser, exhibited speed-dependent anisotropies; the associated $\beta(v)$ is shown in the lower frame of Fig. 5.

To accurately translate this information into a predicted time-of-flight distribution for the experiments using the scattering apparatus, seen in Fig. 6, we then scaled the individual points in the P(v) by $(1 + \beta/4)$to account for the fact that, even with an unpolarized laser, those photofragments with a parallel angular distribution are more likely to be scattered in the detector plane.[29] Figure 6 shows the predicted time-of-flight on the observed signal from the scattering experiments. The fastest peak, appearing just after 200 μs, is well fit by this speed distribution; the fit is shown in solid gray line in the m/e = 79 spectrum. After accounting for the different flight time through the ionizer for the differing mass-to-charge ratios, this signal also appears in the m/e = 15 (CH_3^+) and m/e = 64 (SO_2^+) spectra; these spectra are given in Figs. 11 and

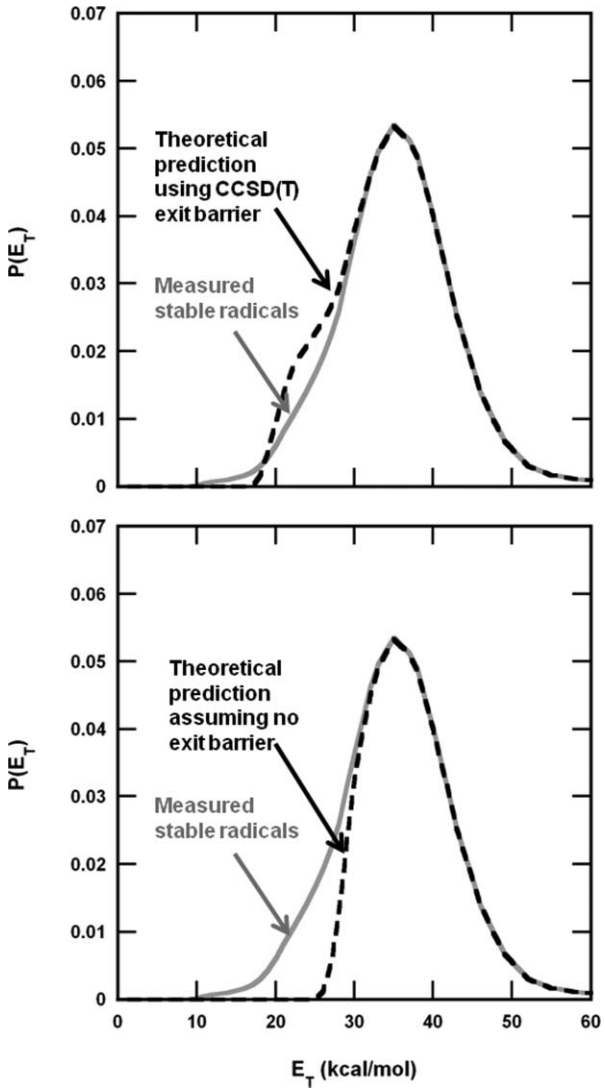

FIG. 3. Predicted and observed total recoil kinetic energy distributions for the stable CH_3OSO radicals formed upon photodissociation at 248 nm. The solid gray line in both the upper and lower frames shows the distribution obtained from the observed signal acquired at m/e = 79 in the imaging experiments; this is discussed in detail in Sec. III D. In Sec. III C, we discussed a method of predicting the stable radical distribution using an impulsive model to calculate the amount of internal energy partitioned into rotation; both the upper and lower frames show the comparison between the prediction (dashed black line), scaled for the relative thermal populations of the two isomers, and the observed signal. The upper frame shows the prediction based on the barrier heights calculated at the CCSD(T) level of theory, and the lower frame shows the predicted fit if the CH_3OSO radicals dissociated to $CH_3 + SO_2$ with no barrier beyond the endoergicity. We note that we were unable to measure the Cl ($^2P_{1/2}$) velocity distribution, so the model does not account for some of the CH_3OSO radicals having 2.5 kcal/mol less internal energy. These distributions do not exhibit a sharp cutoff, as calculated from Eq. (6), because the fits include a thermal distribution of vibrational energies for $E_{precursor}$.

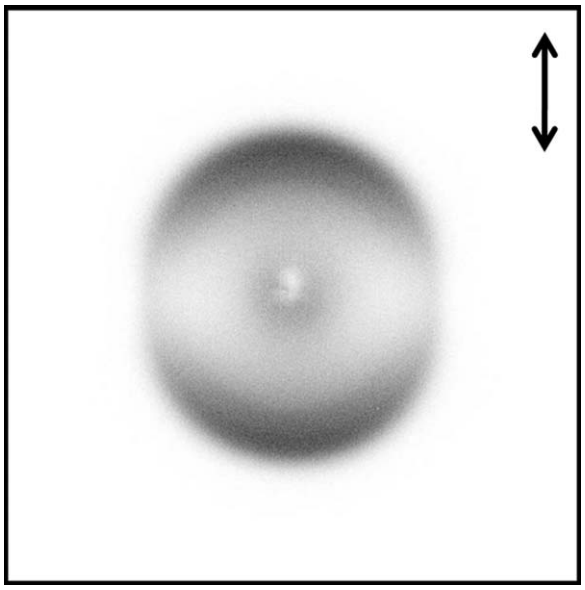

FIG. 4. Raw image of the stable CH_3OSO radicals detected at m/e = 79 (CH_3OSO^+) with 118 nm and accumulated for roughly 50 000 laser shots. The photodissociation laser was polarized in the vertical plane of the image, as shown with the arrow. The image is 731 × 731 pixels and is the result of subtracting the background images obtained with 248 nm only and 118 nm only from the raw data.

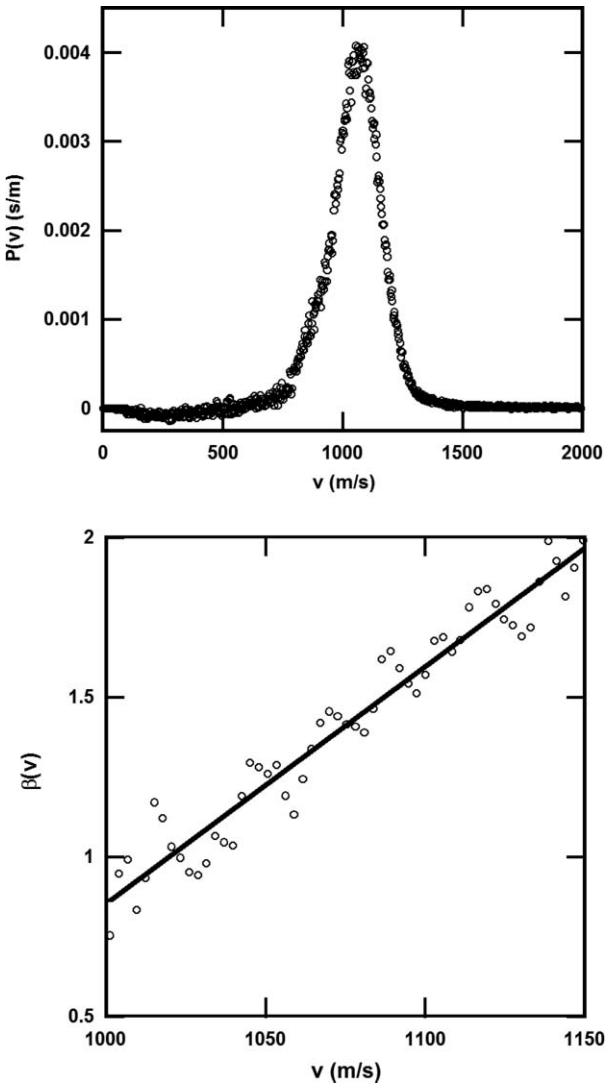

FIG. 5. Speed and anisotropy distributions of the m/e = 79 (CH_3OSO^+) products from the imaging data. The top frame shows the background-subtracted speed distribution of the products detected in the imaging lab at m/e = 79 (CH_3OSO^+) (Fig. 4). The speed-dependent anisotropy is shown in the lower frame. The predicted arrival time of these CH_3OSO ions in the scattering apparatus is given in solid gray line in the m/e = 79 time-of-flight spectrum shown in Fig. 6. Upon 200 eV electron bombardment ionization, these stable radicals also give signal at m/e = 15 (CH_3^+) and at m/e = 64 (SO_2^+); the fits shown in solid gray line in the m/e = 15 (CH_3^+) and m/e = 64 (SO_2^+) spectra (Figs. 11 and 12, respectively) are calculated from this P(v) (upper frame).

12, respectively, and this fit is again shown in solid gray line. The slower signal peaking around 350 μs is fit by the cluster $P(E_T)$ derived from the m/e = 35 (Cl^+) signal shown in the bottom frame of Fig. 1 and discussed in Sec. III B. The signal peaking near 260 μs is not fit by either of these two sources – stable CH_3OSO radicals or clusters. This signal is attributed to the photodissociation of the dimethyl sulfite contaminant ($CH_3OS(O)OCH_3$) and will be discussed in the following subsection.

E. $CH_3OS(O)O$ products from the photodissociation of dimethyl sulfite, $CH_3OS(O)OCH_3$

As mentioned in the Methods section, there was another contaminant, dimethyl sulfite ($CH_3OS(O)OCH_3$), that also underwent photodissociation at 248 nm. The presence of this impurity was confirmed by both ^1H NMR as well as the presence of m/e = 110 signal appearing at the very center of the image in the imaging lab. The ionization energy of this molecule is reported as 9.9 eV;[30] we thus attributed this signal to dimethyl sulfite molecules that were present in the molecular beam, but that did not undergo photodissociation.

The dimethyl sulfite contaminant contributed, at least in part, to signal seen at mass-to-charge ratios common to the $CH_3OS(O)Cl$ precursor. These contributions were most obvious in the m/e = 15 (CH_3^+) spectrum as well as in the m/e = 79 (CH_3OSO^+) spectrum. The main photodissociation products of the dimethyl sulfite contaminant are CH_3 (mass 15) and $CH_3OS(O)O$ (mass 95), the latter of which undergoes dissociative ionization at 200 eV to yield several daughter ions. This portion of the time-of-flight spectra, corresponding to the daughter ions of the mass 95 radical, was separated enough from the time-of-flight signal associated with the $CH_3OS(O)Cl$ photodissociation products, allowing us to fit these portions separately. Specifically, we used the m/e = 79 spectrum taken with electron bombardment ionization (Fig. 6) to obtain a $P(E_T)$ corresponding to the photodissociation of $CH_3OS(O)OCH_3$ to CH_3 + $CH_3OS(O)O$; this was done by forward convolution fitting of the signal that was unfit by either the stable parent CH_3OSO radicals or by clusters, sources which are outlined in Sec. III D. The $P(E_T)$ obtained via this fitting procedure is shown in Fig. 7, and the predicted time-of-flight based on that $P(E_T)$ is shown in dotted black line in the m/e = 79 (CH_3OSO^+) and m/e = 15 (CH_3^+) spectra, Figs. 6 and 11, respectively. We note that daughter ions at m/e = 64 (SO_2^+) may also be present, although the predicted

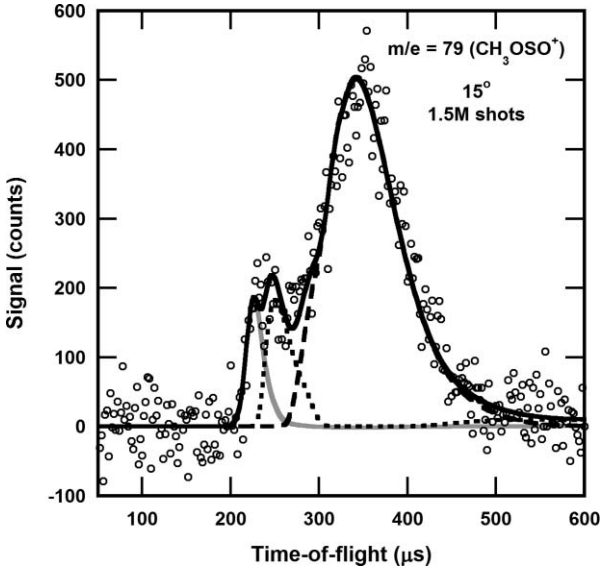

FIG. 6. Time-of-flight spectrum taken at m/e = 79 (CH_3OSO^+) of the products resulting from the photodissociation of methoxysulfinyl chloride. The data are shown in open circles, and the total forward convolution fit to the data (shown in solid black line) is the sum of three contributions. The solid gray line shows the contribution from the primary S-Cl bond fission of methoxysulfinyl chloride resulting in CH_3OSO detected at its parent mass-to-charge ratio; this fit is obtained from the imaging P(v) (Fig. 5) as described in Sec. III D. The dashed black line depicts the signal arising from molecular clusters in the beam. The dotted black line shows the forward convolution fit of the remaining signal – that not fit by stable m/e = 79 radicals or by molecular clusters. This remaining signal, peaking around 250 μs, is attributed to the dissociative ionization of $CH_3OS(O)O$ (mass 95) products from the photodissociation of the $CH_3OS(O)OCH_3$ contaminant in the molecular beam. The $P(E_T)$ used to obtain this fit is given in Fig. 7.

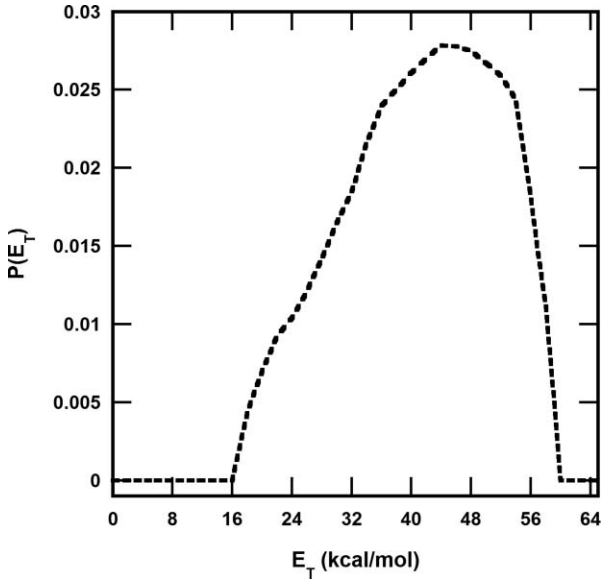

FIG. 7. The total recoil kinetic energy distribution, $P(E_T)$ for the photodissociation of dimethyl sulfite, $CH_3OS(O)OCH_3$ (mass 110), yielding CH_3 (mass 15) and $CH_3OS(O)O$ (mass 95) radicals. This distribution was derived from forward convolution fitting of a portion of the data taken at m/e = 79 (CH_3OSO^+), as shown with dotted black line in Fig. 6. Accounting for flight time through the ionizer, the $CH_3OS(O)O$ parent radical appears at m/e = 15 (CH_3^+) and m/e = 79 (CH_3OSO^+), but not parent m/e = 95 ($CH_3OS(O)O^+$). The momentum-matched CH_3 products were not detected in the imaging experiments; their predicted arrival times are shown in the m/e = 15 time-of-flight spectrum taken with electron bombardment ionization (Fig. 11).

arrival time closely overlaps with the flight time of SO_2 products from the dissociation of vibrationally excited CH_3OSO radicals (see Sec. III F).

The momentum-matched CH_3 products formed in the photodissociation of $CH_3OSO(O)OCH_3$ were not detected. Perhaps they are less subject to being ionized because of the large velocities (3000–5400 m/s) that are imparted to this light cofragment. These velocities would result in the neutral CH_3 products traveling distances on the order of 10^{-4} m before the ionization laser arrives. The ionization laser was fired 40 ns after the photodissociation laser and is tightly focused. We also note that we did not see signal at m/e = 95 ($CH_3OS(O)O$) with the imaging apparatus, even though the ionization energy is calculated to be 9 eV with G3//B3LYP/6-311++g(3df,2p); possibilities for this observation include dissociative ionization and multiphoton events.

F. $CH_3 + SO_2$ products from the dissociation of vibrationally excited CH_3OSO

The CH_3OSO radicals that are formed in conjunction with the slowest Cl atoms are formed with enough vibrational energy to surmount the dissociation barrier to $CH_3 + SO_2$ products. In both the scattering and imaging labs, we saw signal at m/e = 15 (CH_3^+). Similar to the m/e = 79 time-of-flight spectrum obtained in the scattering experiments, the m/e = 15 time-of-flight spectrum was also complicated by other contributing signal sources. These sources include the dissociative ionization of the CH_3OSO radical (mass 79) discussed in Sec. III D, the dissociative ionization of the $CH_3OS(O)O$ (mass = 95) photofragment discussed in Sec. III E as well as the photodissociation of molecular clusters in the beam. The data taken in the imaging lab, using 10.5 eV photoionization, is free from these other contributing signal sources.

Figure 8 shows a representative image taken at m/e = 15 (CH_3^+); we are able to derive from this image a speed distribution for the detected methyl radicals. The imaging data reveal the *net* velocity imparted to the CH_3 products: the vector sum of the velocity imparted to the CH_3OSO radical in the initial S-Cl bond photofission with the velocity imparted when the nascent radical dissociates to $CH_3 + SO_2$, $\vec{v}_{CH_3OSO,1^oS-Cl}+\vec{v}_{CH_3,2^o}$. Thus, we must separately model the velocity imparted in the primary S-Cl bond fission, $\vec{v}_{CH_3OSO,1^oS-Cl}$, and the additional velocity imparted as the radical dissociates to $CH_3 + SO_2$, $\vec{v}_{CH_3,2^o}$, in order to predict the measured net velocities of the momentum-matched CH_3 products. Because we have already determined the distribution of $\vec{v}_{CH_3OSO,1^oS-Cl}$, forward convolution fitting of the CH_3 P(v) allows us to derive the distribution of energies imparted to relative translational energy when the CH_3OSO radicals dissociate to $CH_3 + SO_2$. To calculate the velocities of the dissociating CH_3OSO radicals, we use the portion of the measured S-Cl bond fission $P(E_T)$ shown in dashed gray line in Fig. 2 and discussed in Sec. III B; the velocities predicted by this primary $P(E_T)$ are added to those calculated from the secondary $P(E_T)$, found from the forward convolution fitting

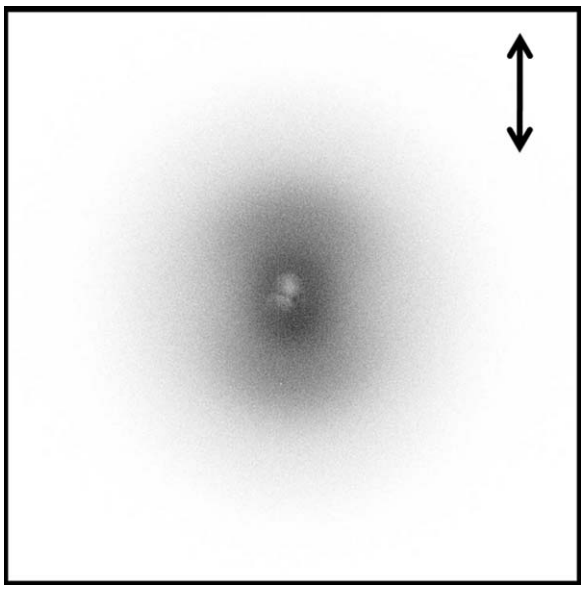

FIG. 8. Raw image of the signal at m/e = 15 (CH_3^+) with 118 nm photoionization and accumulated for roughly 50 000 laser shots. This signal is assigned to CH_3 products from the dissociation of vibrationally excited CH_3OSO radicals. The photodissociation laser was polarized in the vertical plane of the image, as shown with the arrow. The image is 731 × 731 pixels and is the result of subtracting the background images obtained with 248 nm only and 118 nm only from the raw data.

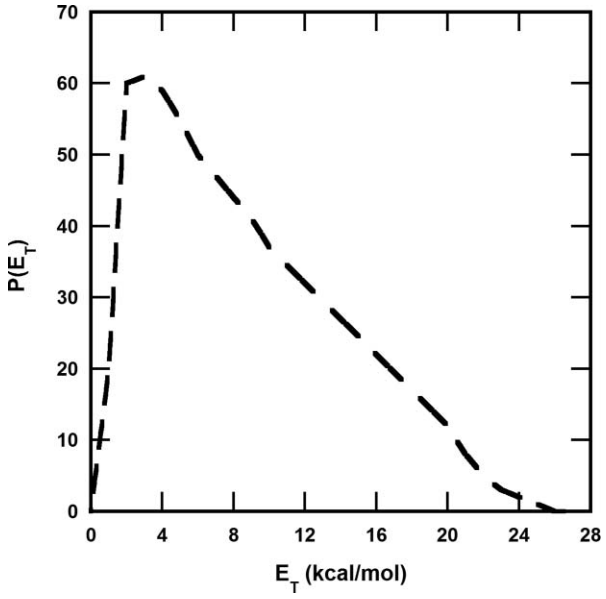

FIG. 10. The recoil translational energy distribution, $P(E_T)$, for the dissociation of vibrationally excited CH_3OSO radicals to $CH_3 + SO_2$. Forward convolution fitting of the data shown in open circles in Fig. 9 was used to derive this $P(E_T)$. For the primary S-Cl bond fission, the low kinetic energy portion of the overall $P(E_T)$ shown in dashed gray line in Fig. 2 was used, as that portion results in CH_3OSO radicals that dissociate. The $P(E_T)$ shown here is used to calculate the additional velocity imparted as the nascent CH_3OSO radicals dissociate to $CH_3 + SO_2$.

of the signal described above, to calculate the fit shown in solid black line and superimposed on the observed speed distribution (open circles) in Fig. 9. The secondary $P(E_T)$, for the dissociation of CH_3OSO to $CH_3 + SO_2$, used to obtain this fit is shown in Fig. 10. For this fitting, we assume both the primary and the secondary dissociations are isotropic.

A fit of the signal observed at m/e = 15 upon electron bombardment ionization is given in Fig. 11. The contributions to that signal include the dissociative ionization of $CH_3OS(O)O$ (mass 95), the dissociative ionization of CH_3OSO (mass 79), and molecular clusters – all described in Secs. III D and III E – along with the secondary dissociation products formed from vibrationally excited CH_3OSO radicals. The latter contribution is derived from the same primary and secondary $P(E_T)$ used to fit the observed methyl speed distribution described above and shown in Fig. 9.

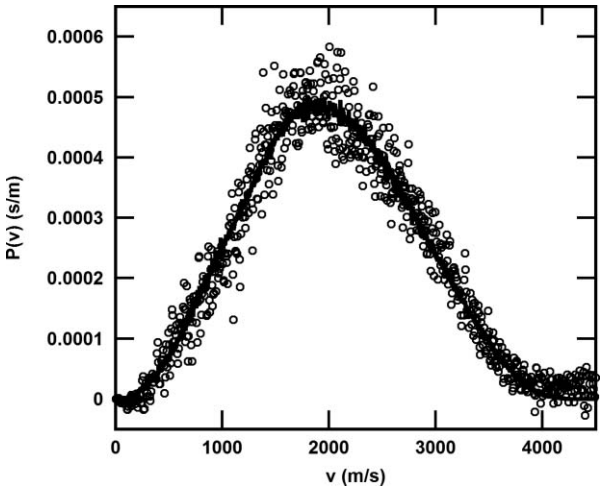

FIG. 9. Speed distribution of the CH_3 products derived from the imaging data in Fig. 8. The open circles represent the background-subtracted speed distribution of the products detected at m/e = 15 (CH_3^+). The solid black line shows the fit obtained by considering the velocities imparted in the primary S-Cl bond fission of $CH_3OS(O)Cl$, followed by those imparted as the vibrationally excited CH_3OSO radicals dissociate to $CH_3 + SO_2$. The secondary $P(E_T)$ used to model the latter dissociation is shown in Fig. 10.

The SO_2 products are formed in conjunction with CH_3 in the dissociation of CH_3OSO radicals. A fit of the signal observed at m/e = 64 (SO_2^+) is shown in Fig. 12. The contributions to that spectrum include dissociative ionization of the mass 79 (CH_3OSO) neutral photofragments to m/e = 64 (SO_2^+), SO_2 products formed from secondary dissociation of those CH_3OSO radicals formed with enough internal energy to surmount the barrier to $CH_3 + SO_2$, and the dissociative ionization of molecular clusters. We use the same $P(E_T)$'s obtained for the methyl signal in the imaging lab to obtain the fit shown in long-dashed gray line in that spectrum. We did not include in this fit the possibility that the mass 95 ($CH_3OS(O)O$) neutral photofragment, formed in the O-C bond fission channel described in Sec. III E, could dissociatively ionize to m/e = 64 (SO_2^+). We ignored this contribution only because that signal closely overlaps with the signal predicted from the distribution of velocities of the SO_2 products formed as the vibrationally excited CH_3OSO radicals dissociate; an alternative fit to the signal peaking just before 300 μs is given in the supplementary material.[14]

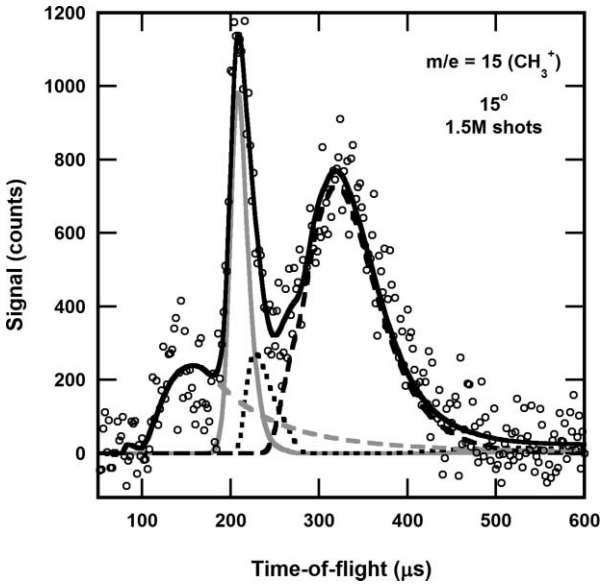

FIG. 11. Time-of-flight spectra taken at m/e = 15 (CH_3^+) with 200 eV electron bombardment detection. The data are shown in open circles, and the overall fit shown in solid black line. The contribution from neutral $CH_3OS(O)O$ photofragments (mass 95) dissociatively ionizing to m/e = 15 is shown in dotted black line, while the stable CH_3OSO radicals (mass 79) dissociatively ionizing to m/e = 15 is shown in solid gray line. The long-dashed gray line is the contribution from CH_3 radicals predicted from the speed distribution obtained from the imaging data (shown in Fig. 9). We assumed an isotropic angular distribution for the secondary dissociation of CH_3OSO to $CH_3 + SO_2$.

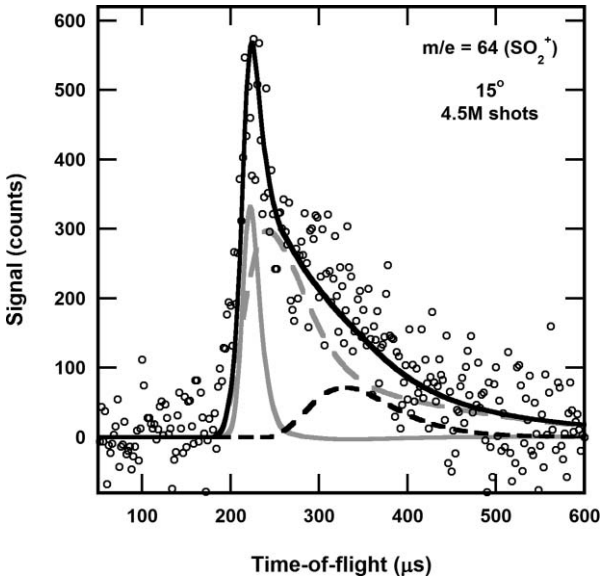

FIG. 12. Time-of-flight spectra taken at m/e = 64 (SO_2^+). The data are shown in open circles, and the overall fit is shown in solid black line. This spectrum contains the contribution from stable CH_3OSO radicals (mass 79) dissociatively ionizing to m/e = 64 as well as the dissociative ionization of molecular clusters in the beam, both upon 200 eV electron bombardment ionization; these fits are shown in solid gray and dashed black line, respectively. The long-dashed gray line is the predicted time-of-flight of SO_2 from the dissociation of CH_3OSO radicals. It is derived using the imaging methyl P(v) shown in Fig. 9.

IV. DISCUSSION

This study resolved the dissociation dynamics of CH_3OSO radicals formed from the photodissociation of $CH_3OS(O)Cl$. Some of the vibrationally excited radicals that were formed dissociated to $CH_3 + SO_2$, a process that partitions substantial energy into recoil translational energy. The measured distribution of recoil kinetic energies in this dissociation, extending beyond 20 kcal/mol, reflects both the high rotational energies of the dissociating radicals and the repulsive forces along the C-S bond after the transition state. This is consistent with the electronic structure results of our collaborator Lau,[4] which show a significant barrier beyond the endoergicity (by 13.9 kcal/mol).

Using the CCSD(T) predicted dissociation barriers of 30.7 and 28.7 kcal/mol for the *syn*- and *anti*-isomers, respectively, we are able to use our impulsive model to roughly predict the measured speed distribution of those surviving CH_3OSO radicals; these radicals were detected at the m/e = 79 parent ion in both the imaging and scattering experiments as well as the m/e = 15 (CH_3^+) and m/e = 64 (SO_2^+) daughter ion in the scattering experiments. This directly supports the reliability of the current CCSD(T) predicted dissociation barrier, which has been done with quadruple-zeta basis sets and incorporating essential relativistic effect and core-valence corrections for the sulfur-containing compounds.

This work also allowed us to show that the photodissociation of $CH_3OS(O)Cl$ proceeds via a single photodissociation channel at 248 nm; unlike our previous experiments on CH_3SO_2Cl,[3] the $CH_3OS(O)Cl$ molecule does not have a methyl-elimination channel that significantly competes with the primary S-Cl bond fission channel. The measurement of SO_2, CH_3, and Cl atom velocity distributions – along with that of the stable CH_3OSO radicals – allowed us to definitively show all of the methyl radical products result from photofission of the Cl bond followed by dissociation of the CH_3OSO co-fragment.

Our data also offer useful results on the photodissociation of dimethyl sulfite, $CH_3OS(O)OCH_3$. A previous publication by Kozlowski *et al.* suggested that the least endothermic channel for the dissociation of dimethyl sulfite would lead to OCH_3 (mass 31) and CH_3OSO (mass 79) products.[31] The authors used thermochemical data to estimate the endothermicity of various photodissociation pathways. They did not, however, even consider the pathway yielding CH_3 (mass 15) and $CH_3OS(O)O$ (mass 95) products. After detecting this channel in our experiments, we performed calculations at the G3//B3LYP/6-311++g(3df,2p) level of theory. Those results show that the pathway leading to CH_3 and $CH_3OS(O)O$ products requires actually 2.4 kcal/mol less energy than the pathway leading to CH_3O and CH_3OSO. The lower endoergicity results, in part, from resonance-stabilization of the $CH_3OS(O)O$ products. We also note that, although these authors presented a UV-vis photoabsorption spectrum of dimethyl sulfite, they only did so for wavelengths between 190 and 225 nm. Although their resulting spectrum seems to imply that the absorption cross section decreases drastically after 190 nm, we note here that we do see significant signal that we can only attribute to the photodissociation of $CH_3OS(O)OCH_3$ at 248 nm.

Note added in proof. Y.-P. Lee sent us a preprint of his work on the IR spectrum of CH_3OSO radicals.[32]

ACKNOWLEDGMENTS

This work was supported by the National Science Foundation, Grant No. CHE-0746050 and the Donors of the American Chemical Society Petroleum Research Fund, Grant No. 47480-AC6. We gratefully acknowledge the help of Ethan Alguire; as an undergraduate, he spent a summer with our group and taught us Professor Fran Blase's synthesis for the photolytic precursor.

[1]M. Speidel, R. Nau, F. Arnold, H. Schlager, and A. Stohl, Atmos. Environ. **41**, 2427 (2007).
[2]A. Saltelli and J. Hjorth J. Atmos. Chem. **21**, 187 (1995).
[3]S. B. Barone, A. A. Turnipseed, and A. R. Ravishankara, Faraday Discuss. **100**, 39 (1995).
[4]B. J. Ratliff, X. N. Tang, L. J. Butler, D. E. Szpunar, and K.-C. Lau, J. Chem. Phys. **131**, 044314 (2009).
[5]B. W. Alligood, B. L. FitzPatrick, E. J. Glassman, L. J. Butler, and K.-C. Lau, J. Chem. Phys. **131**, 004305 (2009).
[6]V. Bossoutrot, A. Kukui, G. Laverdet, and G. Le Bras, J. Phys. Chem. A **107**, 1155 (2003).
[7]A. Ray, I. Vassalli, G. Laverdet, and G. Le Bras, J. Phys. Chem. **100**, 8895 (1996) and earlier references within.
[8]A. Kukui, V. Bossoutrot, G. Laverdet, and G. Le Bras, J. Phys. Chem. A **104**, 935 (2000).
[9]J. C. Owrutsky, H. H. Nelson, and A. P. Baronavski, J. Phys. Chem. A **105**, 1440 (2001).
[10]A. J. Frank and F. Turecek, J. Phys. Chem. A **103**, 5348 (1999).
[11]L. Zhu and J. W. Bozzelli, J. Mol. Struct.: THEOCHEM **728**, 147 (2005).
[12]J. M. L. Martin, J. Chem. Phys. **108**, 2791 (1988).
[13]G. Berti, J. Am. Chem. Soc.**76**, 1213 (1954).
[14]See supplementary material at http://dx.doi.org/10.1063/1.3589273 for ^{1}H NMR spectra of the synthesized $CH_3OS(O)Cl$ product, along with supplemental spectra and fits not given in the main text.
[15]F. Seel, W. Gombler, and R. Budenz, Justus Liebigs Ann. Chem. **735**, 1 (1970).
[16]Y. T. Lee, J. D. McDonald, P. R. LeBreton, and D. R. Herschbach, Rev. Sci. Instrum. **40**, 1402 (1969).
[17]N. R. Daly, Rev. Sci. Instrum. **31**, 264 (1960).
[18]M. Kawasaki, K. Kasatani, H. Sato, H. Shinohara, N. Nishi, H. Ohtoshi, and I. Tanaka, Chem. Phys. **91**, 285 (1984).
[19]G. Baum, C. S. Effenhauser, P. Felder, and J. Robert Huber, J. Phys. Chem. **96**, 756 (1992).
[20]A. Chichinin, T. S. Einfeld, K.-H, Gericke, J. Grunenberg, C. Maul, and L. V. Schäfer, Phys. Chem. Chem. Phys. **7**, 301 (2007).
[21]A. Chichinin, T. Einfeld, C. Maul, and K.-H. Gericke, Dokl. Phys. Chem. **407**, Part 1, 72 (2006).
[22]L.-K. Chu, Y.-P. Lee, and E. Y. Jiang, J. Chem. Phys. **120**, 3179 (2004).
[23]A. J. R. Heck and D. W. Chandler, Annu. Rev. Phys. Chem. **46**, 335 (1995).
[24]A. T. J. B. Eppink and D. H. Parker, Rev. Sci. Instrum. **68**, 3477 (1997).
[25]Y. Sato, Y. Matsumi, M. Kawasaki, K. Tsukiyama, and R. Bersohn, J. Phys. Chem. **99**, 16307 (1995).
[26]Y. Liu and L. J. Butler, J. Chem. Phys. **121**, 11016 (2004).
[27]L. Wang, Y. T. Lee, and D. A. Shirley, J. Chem. Phys. **87**, 2489 (1987).
[28]B. J. Ratliff, C. C. Womack, X. N. Tang, W. M. Landau, L. J. Butler and D. E. Szpunar, J. Phys. Chem. A **114**, 4934 (2010).
[29]L. J. Butler, Ph.D. dissertation, Department of Chemistry, University of California, Berkeley, 1985.
[30]H. Bock and B. Solouki, Chem. Ber. **107**, 2299 (1974).
[31]R. Kozlowski, G. B. Fazekas, M. C. Withiam, K. Bloomer, R. Sampson, T. D. Allston, and G. A. Takacs, J. Photochem. **18**, 117 (1982).
[32]J.-D. Chen and Y.-P. Lee, J. Chem. Phys. **134**, 094304 (2011).